FURTHER INVESTIGATION ON VORTEX TURBULENT CHARACTERISTICS IN PATTERN TRANSITION OF A SFRJ SIMULATOR

S. C. Lee†
Department of Electrical Engineering, Yung Ta Institute of Technology and Commerce
Pingtung, Taiwan 909, Republic of China

ABSTRACT

The present numerical work focuses on vortical structures evolutions of a four-pattern transition in a SFRJ simulator. Four various flow patterns evolve four vortex-pairing mechanisms along shear layer, especially the combinations of two and three contiguous vortices in pattern B. The stretched feedback jetflow gradually forms the small corner eddy after the periodic phase of 225°, and this small corner eddy mixes with the shear layer to evolve into the large corner bubble in the first half of next period. The above two alternative evolutions result in the complicated vortex-paring. Near the reattachment, the deflected fluid decreases with the mass ratio in the time-averaged flow, while the mergence of three successional vortices of pattern B demonstrates the superior performance of instantaneous vortical entrainment.

1. INTRODUCTION

As shown in FIG. 1, $u_i(y)$, U_{max}, δ, and m are respectively the inflow velocity profile, the maximal velocity of inlet mainstream, boundary layer thickness of inlet mainstream, and the fitting constant of inflow velocity profile. The backward facing step flow possesses all characteristics of the separation-reattachment flow field, including the free stream, shear layer, recirculation zone, and redeveloped boundary layer. The applications of bottom wall blowing are simulated in the cooling of SFRJ, electric circuits, turbine blades, and etc. The shedding vortex disturbances relate closely to the evolutions of recirculation bubbles and redeveloped boundary layer. Limited precursors devoted their efforts to explore the mixing effects of wall injection. Eaton and Johnston[1] indicated that the unbalanced momentum inside the main recirculation zone resulted in the fluid low hertz disturbance. Driver and Seegmiller[2] further pointed that the pairing disorders of wavy shedding vortices caused the fluctuations of pressure and velocity.

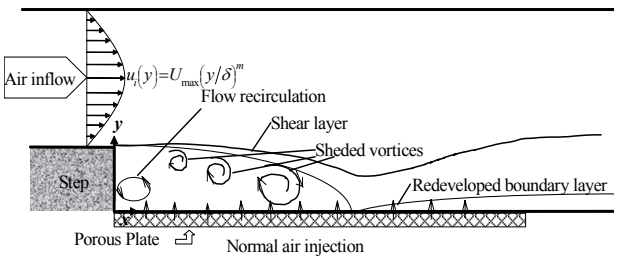

FIG. 1: Schematic Diagram of the Basic Flow Configurations.

Near the reattachment point, Bradshaw and Wong[3] concluded that part of the torn vortex entered the recirculation zone, while the remains moved the downstream. However, Eaton and Johnston[1] observed that most of the large vortices shed to downstream following the recirculation bubble. The numerical results of Chao and Chou[4] revealed that above two kinds of vortical motion were carried on in turn. By varying mass ratio, defined as v_w/U_0, in which v_w and U_0 are respectively the superficial velocity of lateral wall and the mean velocity of inlet mainstream, Ma[5] established the nature of four (A to D) flow structures and mixing mechanisms for a transition from transpiration (Pattern B) to film cooling (Pattern C). Lee[6] numerically reproduced the pattern transition to explore the gas-air mixing. Harinaldi *et al.*[7] experimentally found that the slot injected mass suppressed the velocity, size and detachment of coherent structures.

According to the experiments of Ma[5], the PIV measurements of Huang[8] indicated that two feedback jetflow behaviors induced the evolutions of corner eddy: part of the feedback jetflow evolved into the smaller corner bubble after hitting the step, while the remains mixed upwardly with the shear layer along edge of the larger corner bubble. Nonetheless, the relations between the recirculation bubbles and the vortex-pairing in a periodic evolution are not yet clarified. The blowing effects on transient vortical entrainment are also indefinite in preceding studies. The purpose of the present work is to numerically investigate the large scale vortical transport phenomena in a pattern transition of a backstep flow, as shown in FIG. 1.

2. NUMERICAL STRATEGY

In the present numerical work, the full elliptic transport equations that involved continuity, momentum, and the mixture fraction are expressed in dimensional form as shown in Lee[6].

The full set of transport equations is solved based on discretized equations derived on finite-volume integration over a staggered grid system with refined meshes close to walls and shear layer. The diffusion and convective terms are respectively discretized by means of second-order central differencing and the third-order accuracy QUICK[9] scheme. The second order accuracy Crank-Nicolson scheme is adopted to ensure the iterative stability in time marching. The pressure solver is SIMPLE[10]. Further details of the present method can be found in Chao and Chou[4]. The resultant linear algebraic equations are solved via a line-by-line tridiagonal-matrix algorithm. All the inlet and boundary conditions are collected from the measurements of Ma[5]. A specific near wall treatment[11] with a gas-permeability boundary[6] ensures one's saving on computing cost to approach the real Stokes flow inside the porous plate. The present minimum mesh size (3.34×10^{-3}cm) is finer than the estimated Kolmogorov dissipation scale ($l_d \approx HRe_H^{-3/4} \cong 3.7\times10^{-3}$cm, in which $Re_H=\rho U_0 H/\mu$ is the Reynolds number based on step height H and H=15mm) based on the measurements[5]. All simulations are performed on a non-uniform 165x118 staggered grid system and with a time-step 1.5×10^{-4}s. The settlings of boundary and initial

† Assistant Professor
email: sclee@mail.ytit.edu.tw

conditions adopted here, as well as the verification of the adequacy of the grid and time-step arrangements, can be referred to Lee[6].

3. RESULTS AND DISCUSSION

Simulated results[6] were compared with available time-mean and statistical measurements[5]. The performance of the present work was assessed by that way.

3.1. Observations of the flow fields

The velocity vector plots for flow cases A to D are respectively shown in FIGs. 2(a) to 2(d), in which $\langle u \rangle$ is the time-averaged streamwise velocity. The typical structures of a separation-reattachment flow field can be observed within the region $x \leqq 5H$. Flow case A exhibits the maximal reverse strength contrast to the other cases, while flow case D seems rushing -- that is, all fluid discharges directly toward the downstream. In the flow cases B and C, the suppressed backflow intensities results in fluid stagnation near the step.

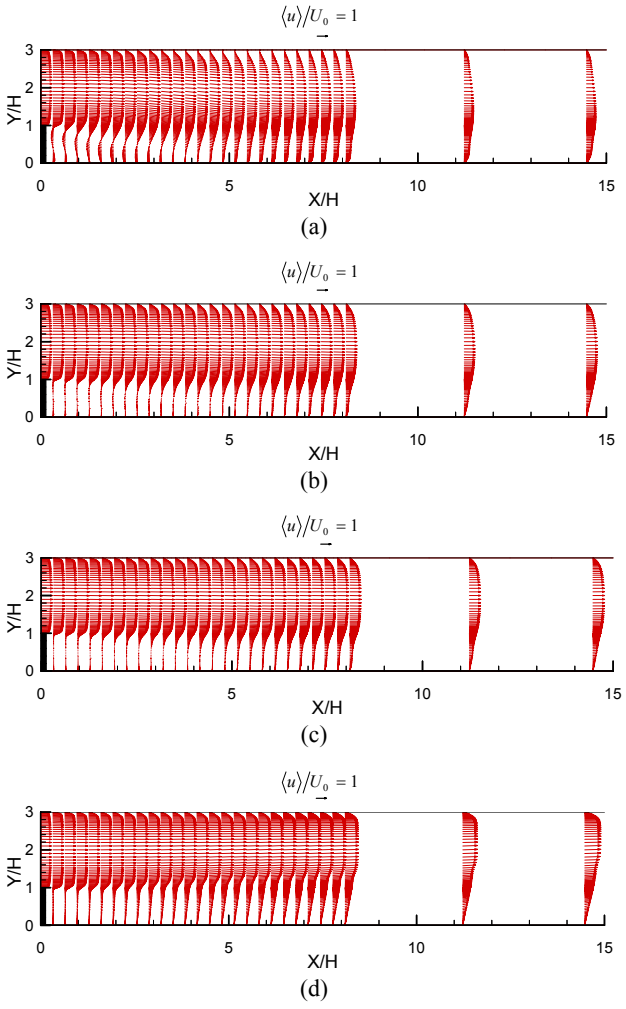

FIG. 2: Vector Plots of Velocity for Flow Cases: (a)A, (b)B, (c)C, and (d)D.

3.2. Periodical vortices dynamics

3.2.1. Pressure spectrums

FIGURE 3 shows the pressure spectrums measured with HP35670A at x=2H, 4H, and 6H about 3mm above the bottom wall. The figure indicates that flow cases A to D exhibit the fundamental frequency of shedding vortex almost within the range of 20 to 21Hz. The specific test cases for variety patterns in this work were collected in TAB. 1.[6]

TAB. 1: The test flow cases.[6]

		Flow patterns									
v_w×100(m/s)		0	3.4	4.8	6.8	8.2	10.2	11.6	13.6	15.0	17.0
U_0[a] (m/s)	2.1	A	B	B	C	C	C	D	D	D	D[e]
	2.6	A	B	B	B	C	C	C[d]	C	D	D
	2.9	A[b]	A	B	B[c]	B	B	C	C	D	D
	3.2	A	A	A	B	B	B	B	C	D	D

[a]Inlet mean velocity.
[b]Test case for flow pattern A.
[c]Test case for flow pattern B.
[d]Test case for flow pattern C.
[e]Test case for flow pattern D.


HP35670A Signal Analyzer[14]

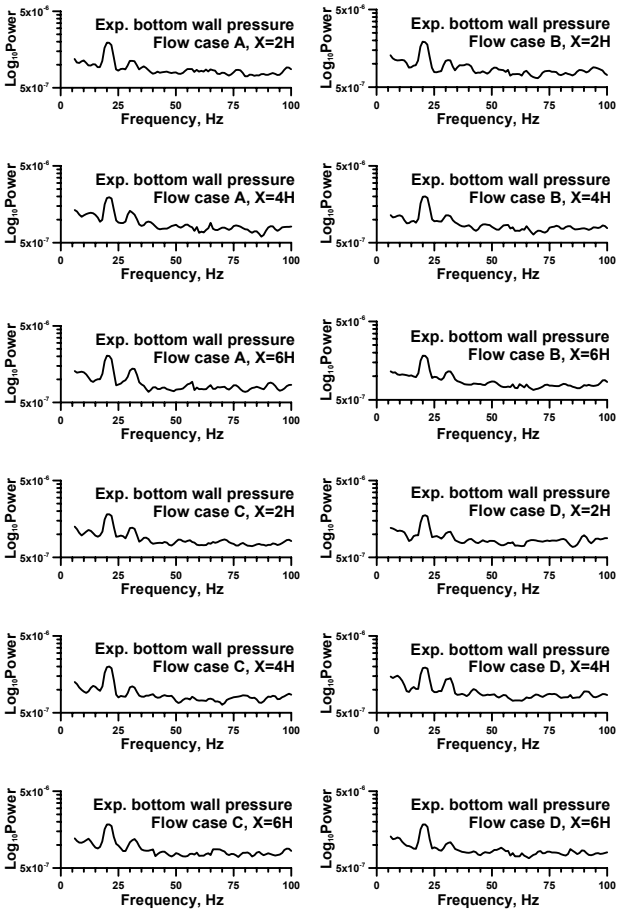

FIG. 3: Bottom Wall Pressure Spectrums Measured by HP35670A Signal Analyzer at x=2H, 4H, and 6H for Flow Cases A, B, C, and D.

For the flow cases A to D, the corresponding inlet Reynolds numbers based on the step height are all below 3000, and the Strouhal numbers, defined as $St_H=f_0H/U_0$[12], are between 0.15 and 0.1. As the results of inlet Reynolds number below $6x10^4$, the vortex shedding frequency subject almost insensibly to wall bleeding and increases linearly with inlet flow velocity. The similar trends were found in the measurements of Yang *et al*.[13] Due to the minute variance of shedding frequency among the flow cases A to D and the coarse resolution of pressure disturbance near the bottom wall, the perturbation of velocity versus pressure spectrum is recalculated as shown in FIG. 4.

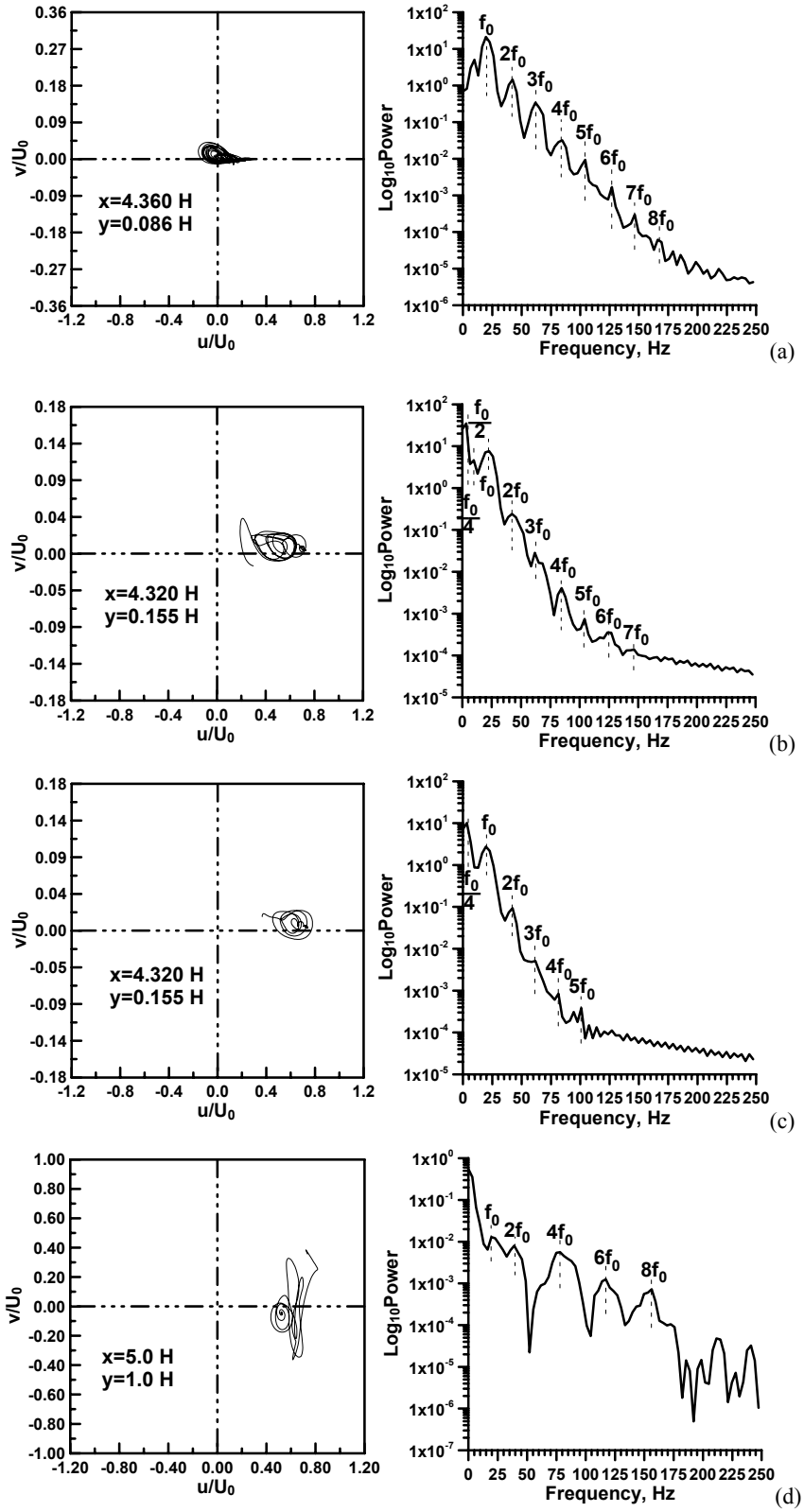

FIG. 4: u/U_0 Spectrum of the Phase of u/U_0 Versus v/U_0 at (x, y) = (a) (4.360H, 0.086H), (b) (4.320H, 0.155H), (c) (4.320H, 0.155H), and (d) (5.0H, 1.0H) for Flow Cases A, B, C, and D, Respectively.

For flow cases A to D, the fundamental frequencies (f_0) of shedding vortex, which decrease gradually with the enhancement of wall mass ratio, are respectively 21, 20.8, 20.2, and 19.5Hz. Such tendencies were shown in the experimental works of Yang *et al*.[13] and Su[14]. The higher harmonics frequencies (nf_0, n = 2, 3, 4…) are identified clearly in the flow cases A, B, and C, while flow case D exhibit harmonics frequencies 2nf_0 (n = 1, 2, 3, 4…) that consists with the measurements of Chen[15]. FIGURE 4(a) shows that the fundamental (f_0) and the higher harmonics frequencies (nf_0, n = 1, 2, 3, 4…) are the intrinsic frequencies of a separation-reattachment flow field, as indicated in the numerical results of Soong *et al*.[16]

Below the dominant frequency f_0, a power peak at about f_0/2 can be identified as the first sub-harmonic frequencies of flow case A, while the velocity spectrum near the bottom wall of the reattachment of flow case B shows the first (f_0/2) and second sub-harmonics (f_0/4). For flow case C, FIG. 4(c) indicates that the dominant frequency is the second sub-harmonic f_0/4 at the position of (x, y) = (4.320H, 0.155H). None of the sub-harmonics appear to be the power peaks in the velocity spectrum of flow case D. The two sub-harmonics relate closely to the dynamic vortical behaviors as depicted follows.

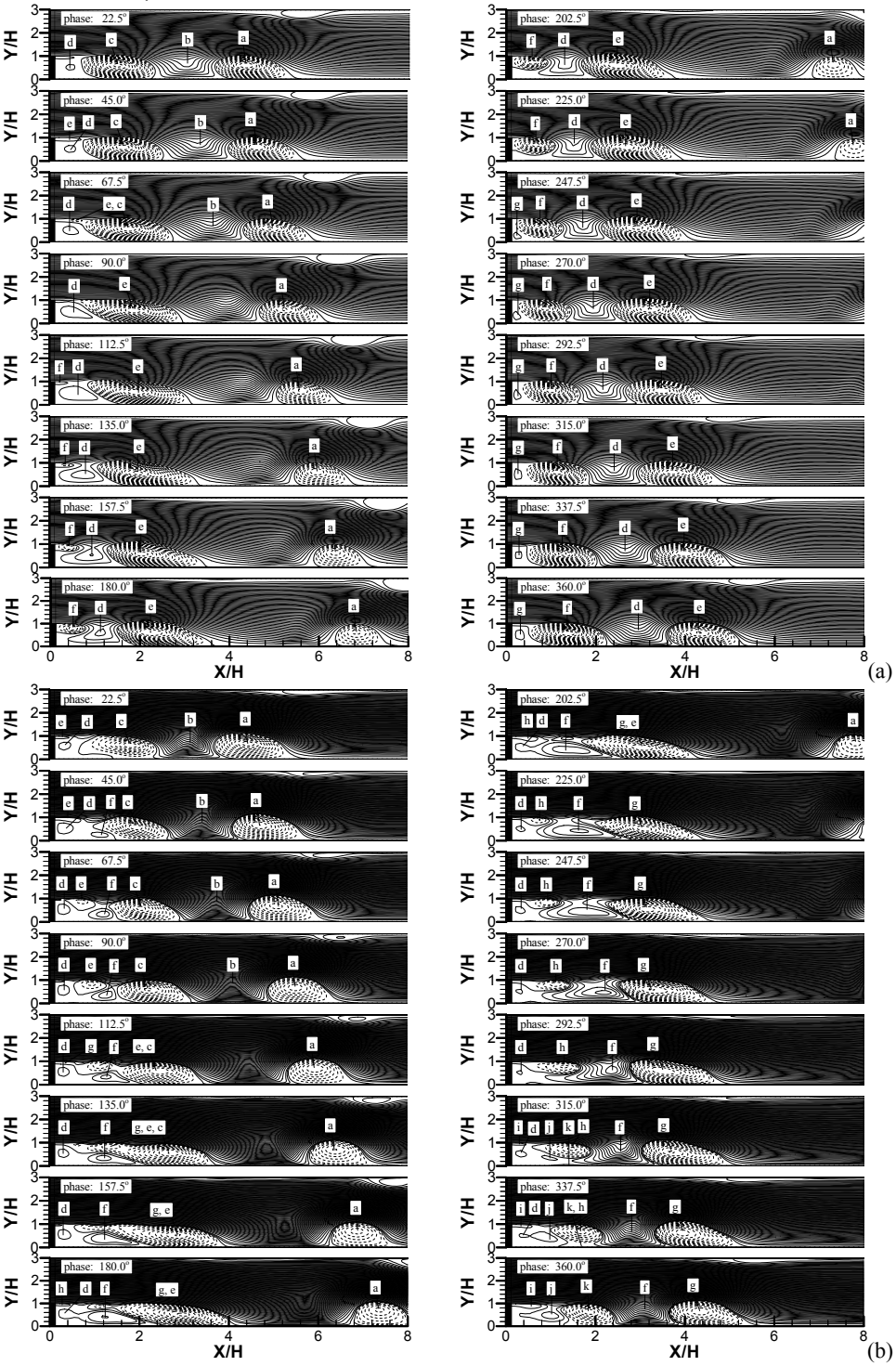

FIG. 5: Full Cycle Evolution of Stream Function for Flow Cases (a)A, (b)B, and (c)C, and Sequences of Vorticity of the Developing Flow Case (d)D from t_+=251.429 to 261.944.

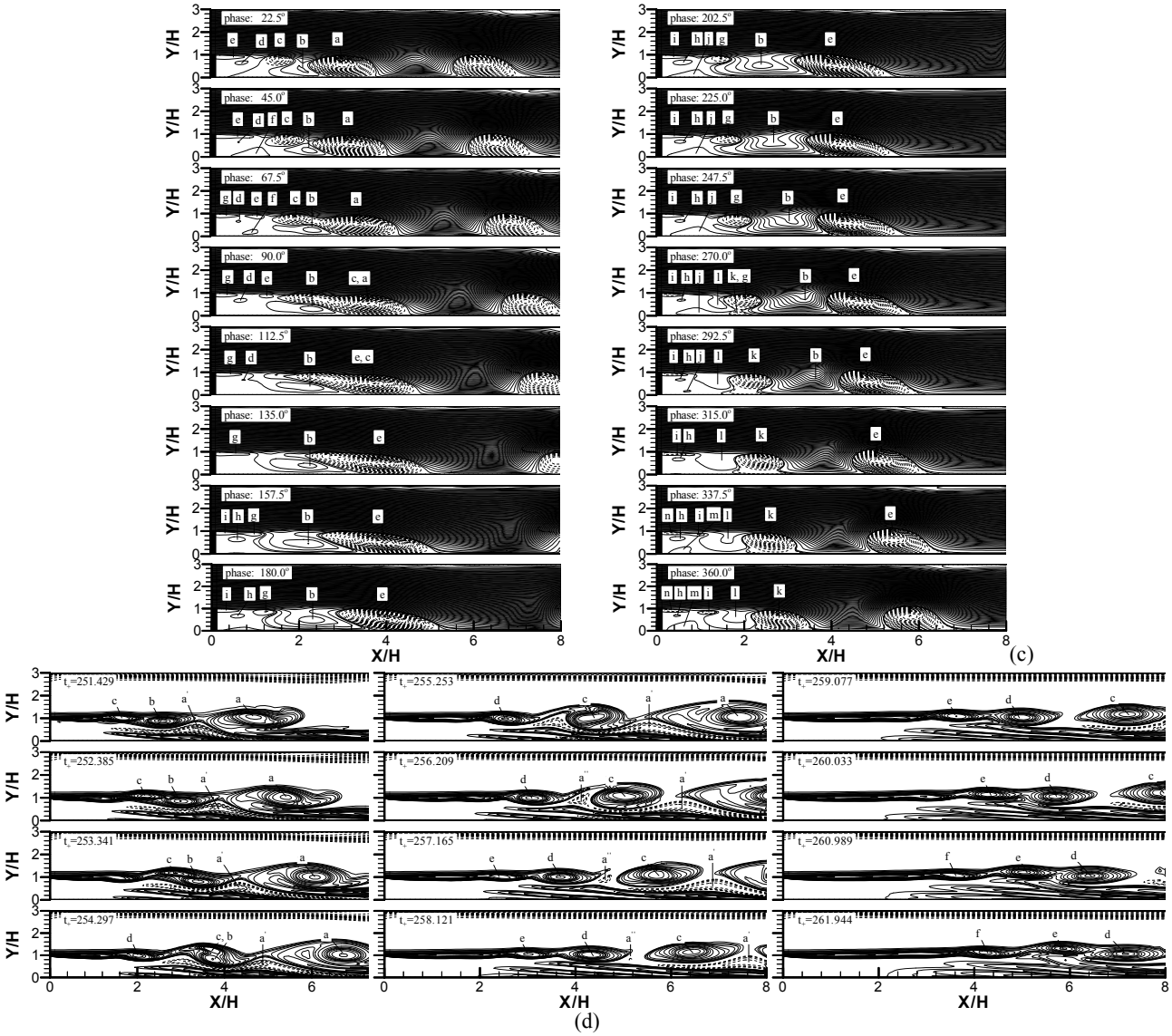

FIG. 5: (cont.)

3.2.2. Large scale vortical evolutions

The time elapsed in a periodic evolution is about 0.048s, which corresponds to a cyclic phase of 360°. For flow cases A to D, FIG. 5 shows the vortex-pairing along the shear layer. In addition to the mergence of two adjacent vortices in both flow cases A and B, flow case B behaves the combination of three continuous vortices (for ex., vortices *c*, *e*, and *g*, between phases 90° and 225°.). Flow case C exhibits the similar merging of three vortices (for ex., vortices *a*, *c*, and *e*, between phases 22.5° and 135°.) as indicated in flow case B. For flow case D, the instantaneous oscillations are plotted instead of periodic vortex-evolution, since the mixing layer vortices are getting weaker in vorticity and less organized downstream x=8H. FIG. 5(d) reveals that pressure feedback results in the pairing of vortices *b* and *c* between stages t_+=252.385~255.253, in which $t_+=tU_0/H$ is the non-dimensional time.

As shown in FIG. 5(a), the shedding vortices *a* and *c* respectively induce the counterclockwise vortices *b* and *d* at phase 22.5°. The shedding vortex *c* induces gradually the feedback jetflow from phases 22.5° to 45°. After hitting the step, the feedback jetflow mixes with the shear layer to develop the induced vortex *d* between phases 45° and 135°. Flow case B involves two small bubbles inside the secondary recirculation zone[6]. FIGURE 5(b) shows that vortex *d* of the periodic flow actually plays the role of the one near the step, while vortex *f* and the eddy *j*, which merges with vortex *d* after phase 315°, evolve into another. In addition to the interchange of mass between vortex *d* and inlet mainstream, vortices *d* and *f* intermix diffusively and the merged vortex *j* interacts upwardly with shear layer. The above evolutions illuminate the interaction between the larger corner bubble and feedback jetflow[8]. FIGURE 5(a) indicates that vortex *f* in flow case A grows up gradually during the second half of periodic oscillation to induce the feedback jetflow. After hitting the step, the feedback jetflow evolves into the smaller corner eddy, as depicted in the observations of Huang[8]. For flow case B, FIG. 5(b) shows the similar vortical behavior between phases 225° and 337.5°.

Because the continuity of mass, the small counterclockwise rotating eddy that adheres to the main recirculation bubble in flow case C is a logical expectation. The vortical dynamics clarify the sequence of such a small eddy. As shown in FIG. 5(c), the combination of three vortices induces the narrower counterclockwise rotating eddy than the one of flow case B, and the stronger mass ratio raises the shedding vortex *k* away from

the bottom wall at phase 315° contrast to the similar evolution of vortex *g* in flow case B between phases 337.5° and 360°. Such trends contribute to the completely development of the counterclockwise rotating vortex *b*.

3.2.3. Instantaneous vortical entrainment

The vortical aspect ratios, defined as r_l/r_s, in which r_l and r_s are respectively the long and short half axes of vortical fitting ellipse, and elliptoid areas in a periodic evolution for the flow cases A to C are respectively shown in FIGs. 6(a) to 6(c). Notice that x_r, x_m, x_{2c}, and x_{3c} in FIG. 6 represent respectively the measured mean reattachment length (4.45*H*), the location of two adjacent eddies the first time to contact with each other, the position of a paring vortex to touch with the bottom wall, and the impingement point on the bottom wall of the merging of three contiguous vortices. For the flow cases A, B, and C, the figure indicates that the locations of x_m are respectively near 0.75*H*, 1.45*H*, and 2.6*H*. The points of x_{2c} are respectively estimated at 1.67*H* and 2.25*H* for the flow cases A and B, while the approximate positions of x_{3c} for the flow cases B and C are respectively 3.2*H* and 4.0*H*.

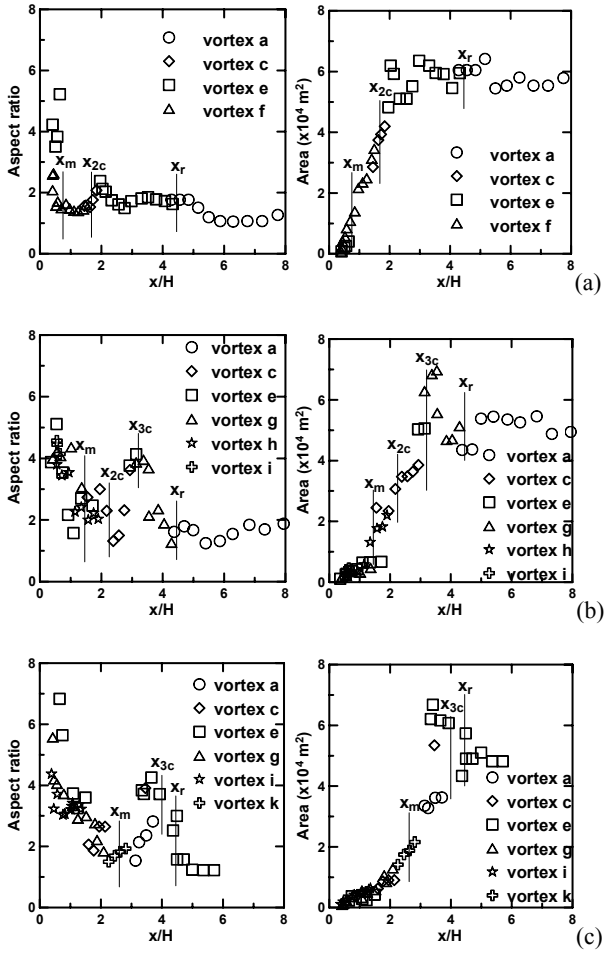

FIG. 6: Evolutions of the Vortical Aspect Ratio and Area in a Full Cycle Motion for the Flow Cases (a)A, (b)B, and (c)C.

For the flow cases A, B, and C, the slenderness of shedding vortex upstream the reattachment point increases with enhancement of mass ratio. In this region although the estimated vortical aspect ratios exhibit ruleless, the pairing of vortices expands the elliptoid aspect ratios, especially the evolutions of three merging vortices in flow cases B and C, as shown in FIGs. 6(b) and 6(c). The fitting elliptoid areas reveal that the entrainments of vortices increase linearly before vortical combinations but decrease with intensity of mass ratio. During the merging of three contiguous vortices, flow case B behaves the superior performance in vortical entrainment with about 7cm^2 fitting area. Near downstream the reattachment point, the vortical entrainments of flow cases A, B, and C decrease with the substantiation of mass ratio, which consist with the time-averaged flow results of Yang *et al*.[17]

4. CONCLUSIONS

On periodic votical evolutions for various flow cases, the present work numerically predicates not only the breakthroughs in conventional sense of the interaction between the shear layer and lateral injection but also the reasons of formation of the specific flow structures.

The mergence of two contiguous vortices can be observed in the flow cases A and D, while flow case C exhibits only the combination of three successional vortices. Flow case B even behaves both above two mergings of shedding vortices. Such complicated vortex-pairing behaviors are mainly due to the smaller corner bubble formed by feedback jetflow during the second half cycle evolves with shear layer into the larger corner eddy almost in the first half of the next period.

Near upstream the reattachment point, the promotion of lateral mass ratio squeezes flatly the shedding vortices. The mergence of contiguous shedding vortices increases the aspect ratio of combining vortices. The combination of three successional vortices in flow case B exhibits the superior performance of transient votical entrainment after hitting the lateral wall.

5. ACKNOWLEDGEMENTS

The experimental works of Dr. Ma Wang-June and Mr. Su Yu-Chieh are much appreciated.

6. REFERENCES

[1] J. K. Eaton, J. P. Johnston,
A Review of Research on Subsonic Turbulent Flow Reattachment, AIAA J., 1981, Vol. **19**, No. 9, pp. 1093-1100.

[2] D. M. Driver, H. L. Seegmiller,
Time Dependent Behavior of a Reattaching Shear Layer, AIAA J., 1987, Vol. **25**, No. 7, pp. 914-919.

[3] P. Bradshaw, F. Y. F. Wong,
The Reattachment and Relaxation of a Turbulent Shear Layer, J. Fluid Mech., 1972, Vol. **52**, No. 1, pp. 113-135.

[4] Y. C. Chao, W. F. Chou,
SIMPLER-based Procedure for Numerical Simulation of Dynamic Vortical Characteristics of Some Turbulent Flows, Numer. Heat Transf. B, 1998, Vol. **33**, No. 1, pp. 37-64.

[5] W. J. Ma,
Transpiration Cooling Phenomena in Separated Flow Field, Ph. D. Thesis, Department of Power Mechanical Engineering, National Tsing Hua Univ., Taiwan, 2000.

[6] S. C. Lee,
Simulation on Transition of Gas-Air Mixing Pattern in a Backward-Step Flow with Lateral Wall Injection, Bulletin of YTITC, 2006, Vol. **6**, No. 2, pp.103-113.

[7] Harinaldi, T. Ueda, M. Mizomoto,
Effect of Slot Gas Injection to the Flow Field and Coherent Structure Characteristics of a Backstep Flow,

Int. J. Heat Mass Transfer, 2001, Vol. **44**, No. 14, pp. 2711-2726.

[8] H. H. Huang,
Transient Flow Structure of Shear Layer over a Backward-Facing Step, M. S. Thesis, Department of Power Mechanical Engineering, National Tsing Hua Univ., Taiwan, 2004.

[9] B. P. Leonard,
A Stable Accurate Convective Modelling Procedure based on Quadratic Upstream Interpolation, Comp. Meth. Appl. Mech. Eng., 1979, Vol. **19**, No. 1, pp. 59-98.

[10] S. V. Patankar,
Numerical Heat Transfer and Fluid Flow, Hemisphere, Washington DC, 1980, pp. 79-138.

[11] S. C. Lee, J. T. Yang, Y. C. Chao,
An LES-Wall Model for Turbulent Back-Step Flow with Wall Transpiration and Pressure Gradient, J. Chin. Soc. Mech. Eng., 2002, Vol. **23**, No. 2, pp. 577-588.

[12] A. S. Ramamurthy, R. Balachandar, H. S. G. Ram,
Some Characteristics of Flow Past Backward Facing Steps Including Cavitation Effects, J. Fluids Eng., 1991, Vol. **113**, No. 2, pp. 278-284.

[13] J. T. Yang, B. B. Tsai, G. L. Tsai,
Separated-Reattaching Flow over a Backstep with Uniform Normal Mass Bleed, J. Fluids Eng., 1994, Vol. **116**, No. 1, pp. 29-35.

[14] Y. C. Su,
Transient Phenomena of Transpiration Cooling in High-Temperature Separated Flow Field, M. S. Thesis, Department of Power Mechanical Engineering, National Tsing Hua Univ., Taiwan, 2001.

[15] Y. J. Chen,
Flow Patterns of High-Temperature Separated Flow with Transpiration Cooling, M. S. Thesis, Department of Power Mechanical Engineering, National Tsing Hua Univ., Taiwan, 2000.

[16] C. Y. Soong, P. Y. Tzeng, C. D. Hsieh,
Numerical Investigation of Flow Structure and Bifurcation Phenomena of Confined Plane Twin-Jet Flows, Phys. Fluids, 1998, Vol. **10**, No. 11, pp. 2910-2921.

[17] J. T. Yang, S. C. Lee, C. Y. Chao,
Analysis of Entrainment in a Sudden-Expansion Channel with Wall Mass Transfer, J. Propuls. Power, 2003, Vol. **19**, No. 3, pp. 514-516.